Engineering Geology 162 (2013) 1–13

Contents lists available at SciVerse ScienceDirect

Engineering Geology

journal homepage: www.elsevier.com/locate/enggeo

Modeling cracking behavior of rock mass containing inclusions using the enriched numerical manifold method

Zhijun Wu, Louis Ngai Yuen Wong *

School of Civil and Environmental Engineering, Nanyang Technological University, Block N1, Nanyang Avenue, Singapore 639798, Singapore

ARTICLE INFO

Article history:
Received 25 January 2013
Received in revised form 8 April 2013
Accepted 2 May 2013
Available online 14 May 2013

Keywords:
Numerical manifold method
Partition of unity method
X-FEM
Crack initiation criterion
Crack evolution technique
Stiff/weak inclusions

ABSTRACT

In this study, the effects of weak and stiff circular inclusions on the overall mechanical behavior, in particular the cracking processes (crack initiation, propagation and coalescence) of a rectangular rock mass under uniaxial compression are investigated. The enriched method, which has been adopted by XFEM to treat the material interfaces, is incorporated into the numerical manifold method (NMM). By incorporating the modified Mohr–Coulomb crack initiation criterion and the crack evolution techniques, the cracking processes of specimens containing either one or two inclusions are successfully modeled by the developed NMM. Comparing the simulation and physical test results, the feasibility of the enriched method in treating inclusions is discussed.

1. Introduction

Inclusions are commonly found in natural materials such as rocks, as well as man-made structure materials such as concrete. It is highly worthwhile to investigate the effects of these inclusions on the overall behavior (weakening or strengthening) of the materials, in particular the cracking process (crack initiation, propagation and coalescence) which usually finally leads to the failure of the structures such as slope sliding and rock fall. Despite that cracks and inclusions are both treated as discontinuities in the medium, the nature of these two discontinuities are different. The first one is obvious and denoted as "strong discontinuity". The latter is not obvious (the displacement field is continuous but the stress and strain are discontinuous) and denoted as "weak discontinuity". Hence, the treatment of these discontinuities in numerical modeling is of great interest.

In general, the crack paths are not known a priori, which makes it impossible to construct a mesh that conforms to the crack path. Therefore, to accurately reproduce the gradual transition from a continuous or weak discontinuous matter to a strong discontinuous matter is not straightforward.

Through the refined mesh near the crack tip and continual remeshing, the classical Finite Element Method (FEM) was successfully used to model crack propagation problems (Rashid, 1998; Trädegård et al., 1998; Bouchard et al., 2003). However, this implementation requires the crack to coincide with the finite element mesh, which complicates the meshing task. Remeshing, which can cater for the crack evolution, however makes the modeling of an arbitrary crack growth in FEM very difficult and time expensive. The meshless method is an alternative attractive method which can alleviate difficulties related to mesh generation and remeshing associated with FEM. Since no remeshing is required, the approach is very attractive for moving boundaries and strong discontinuous problems. Based on the moving least squares approximation, the Element-Free Galerkin (EFG) method (Belytschko et al., 1994) and Element-Free Particle method (EFG-P) (Rabczuk and Belytschko, 2004; Rabczuk et al., 2007) have been successfully applied to model both simple and complicated crack problems. However, the difficulties in enforcing essential boundary conditions and numerical integration, as well as the high computational expense, discourage the meshless method from being widely used.

Recently, a variety of methods have been developed on the basis of the partition of unity method (PUM) (Melenk and Babuska, 1996) for they can explicitly represent discontinuities in the approximation field without further remeshing and assumptions. Among methods building on the PUM based on the FEM, the Extended Finite Element Method (XFEM) (Belytschko and Black, 1999; Moes et al., 1999; Belytschko et al., 2001) and the Generalized Finite Element Method (GFEM) (Strouboulis et al., 2000a,b) are the two widely developed methods. By including additional enriched functions to the standard FEM polynomial approximation field, both of them can successfully capture the

* Corresponding author. Tel.: +65 6790 5290; fax: +65 6791 0676.
E-mail address: lnywong@ntu.edu.sg (L.N.Y. Wong).

0013-7952
http://dx.doi.org/10.1016/j.enggeo.2013.05.001

jumps and singularities across the discontinuities. However, when the problems become more complicated, such as crack branching and multiple crack intersection problems, to define the enrichments of the approximation space will be challenging.

Numerical Manifold Method (NMM) (Shi, 1991, 1992; Babuska and Melenk, 1997), which is also based on the PUM, is another potentially attractive method for discontinuous problems. It combines the widely used FEM and joint or block oriented Discontinuous Deformation Analysis (DDA) (Shi and Goodman, 1989) in a unified form. The unique and superior features of the NMM for the crack analysis include: (1) With the contact technique, large displacement sliding, shearing and even discrete blocky movement are allowed; (2) By simply cutting the mathematical cover by the discontinuity(crack), the discontinuity will be captured without further requirement of incorporating step/jump functions; (3) The discontinuity representation algorithm employed is suitable for any number and any geometrical complexities like intersections, junctions and branching of discontinuities in the element; (4) Using the simplex integration method, element subdivision for the numerical integration of weak form can be avoided in most of the cracked elements.

Due to the capabilities of NMM in dealing with discontinuous problems, NMM has been successfully used for modeling both strong discontinuous problems (Tsay et al., 1999; Chiou et al., 2002; Ning et al., 2011; Wu and Wong, 2012) and weak discontinuous problems (Terada et al., 2007; Kurumatani and Terada, 2009; Wu and Wong, 2013; Wu et al., 2013). However, in previous work, the weak discontinuities are treated the same as strong discontinuities except for the enforcement of the additional displacement compatibility condition along the interface. In the present work, the enriched method as adopted by An et al. (2011) and Nielsen et al. (2012), which can conveniently treat the material discontinuities, is proposed to handle the material interfaces (weak discontinuities) within the NMM framework. Based on the crack initiation and propagation criteria, the crack identification method and the crack evolution technique developed in our previous studies (Wu and Wong, 2013; Wu et al., 2013), the crack mechanism (tensile or shear), the cracking processes and the final failure patterns in the specimens containing single or double inclusions under uniaxial compression are investigated by the developed NMM. The feasibility of the proposed enriched method for simulating the material discontinuities is discussed by comparing the numerical results with the theoretical and laboratory test results.

2. Modeling discontinuities by NMM

The core and most innovative feature of the NMM is the adoption of a two cover (mesh) system, from which the nodes and elements are generated. Similar to other PUMs, the finite covering of a problem domain is also the basic construction of the NMM. In the following subsections, the fundamental knowledge of the NMM, including how the discontinuities (strong and weak discontinuities) are modeled in the NMM, as well as the crack initiation criterion are described. The detailed knowledge of the NMM such as the construction of a finite covering system, the building of partition of unity functions and the application of the simplex integration can be found in Lin (2003).

2.1. The finite cover systems in the NMM

The finite cover systems employed in the NMM are referred to the mathematical cover (MC) and physical cover (PC), respectively (Shi, 1991). The MC, which is used for building PCs, can be either a mesh of regular pattern or a combination of some arbitrary figures. However, the whole mesh has to be large enough to cover the whole physical domain. The physical mesh, which includes the boundary of the material, joints, cracks, blocks and interfaces of material zones, is a unique portrait of the physical domain of a problem, and defines the integration fields. The intersection of the MC and the physical mesh, or the common area of the two systems, defines the region of the PCs. A common area of these overlapped PCs corresponds to an element in the NMM.

Fig. 1 illustrates the basic construction procedures of the finite covering system adopted in the NMM. As illustrated in the figure, the hexagonal MCs first form from the triangular mathematical meshes, such as MCs M_1, M_2, M_3 and M_4. From the formed MCs and the physical meshes the PCs are defined. For example, MC M_1 intersecting with the physical boundary Γ_u forms PC P_1, and MC M_4 intersecting with the crack boundary forms PCs $P^1{}_4$ and $P^2{}_4$, while the common area of the MC and physical mesh forms the PCs P_2 and P_3. Finally, the NMM elements are created by overlapping these PCs, such as the element E_1 forms from the overlapping of PCs P_1, P_2 and P_3.

On each PC P_i, a local displacement functions $u_i(x)$ is independently defined. Then, by the weighting function mentioned in Shi (1991) (the same as PU function), the local displacement functions can be connected together to form a global displacement function for each manifold element as follows:

$$u(x) = \sum_{i=1}^{n} \varphi_i(x)\, u_i(x) \tag{1}$$

where $\varphi_i(x)$ is the weighting functions, which satisfies

$$\varphi_i(x) \geq 0, \quad \forall x \in P_i; \quad \varphi_i(x) = 0, \quad \forall x \notin P_i$$

with

$$\sum_{x \in P_i} \varphi_i(x) = 1.$$

The characteristics of the weighting functions depend on the shape of the mathematical mesh and the order of the displacement approximation field. In this paper, a regular triangular mesh and a linear displacement approximation filed are adopted. The weighting functions then become equal the three node triangular finite element shape functions.

2.2. Criterion for crack initiation

One cannot predict the path of the crack propagation without the crack initiation criterion, which is required to judge whether the crack will propagate at each step. If propagation is indicated, the crack propagation direction and propagation distance have to be determined.

Hitherto, several crack initiation criteria have been proposed, such as the maximum circumferential tensile stress (MTS) (Erdogan and Sih, 1963), the maximum energy release rate (Hussian et al., 1974), the minimum strain energy release rate (Sih, 1974), the principle of local symmetry (Cotterell and Rice, 1980), etc. A detailed summary of the criteria was provided by Khan and Khraisheh (2000). However, these criteria are only suitable for the crack initiation from the pre-existing cracks and the mode I stress intensity factor, $K_I \geq 0$. For cracks initiated from the intact mass or cracks, in which K_I is not applicable, a new criterion is needed.

The Mohr–Coulomb criterion with a tensile cut-off (Brady and Brown, 1993), which is based on the premise that the crack initiation depends on the local stress relative to the strength of material rather than on the stress intensity factors, is adopted. The tensile crack initiation stress and direction are assumed to be related to the maximum tangential tensile stress. Additionally, the shear crack initiation stress and direction can be determined by the material strength parameters (cohesion C and frictional angle ϕ) and the stress status in the elements. The detailed procedures of determining the initiation stress and initiation angle can be found in our previous work (Wu and Wong, 2012).

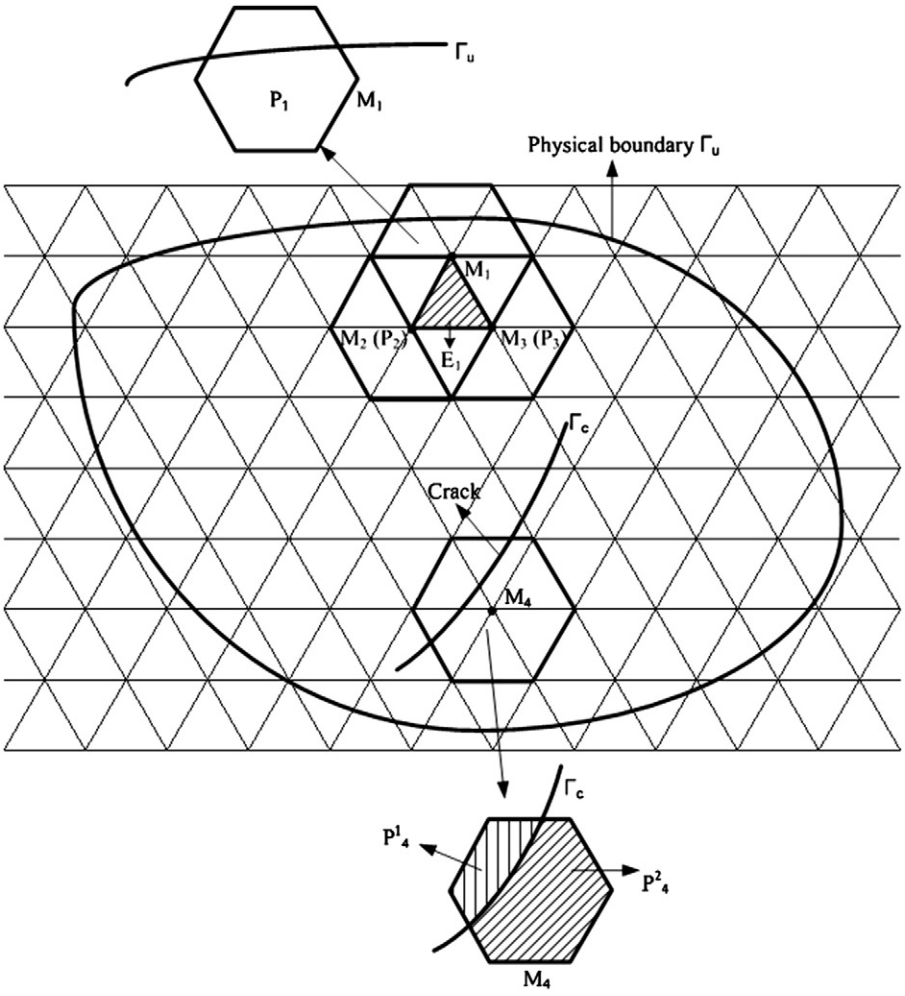

Fig. 1. PCs and manifold elements formed from regular hexagonal MCs defined by the intersection of the MCs with the physical boundaries.

2.3. Algorithm for strong discontinuity (crack) and its transition

As described earlier, the most advanced feature of the NMM is the adoption of two covers to describe a problem. Unlike the enriched functions used in XFEM and GFEM, in which a prior definition of the enrichment functions is required to capture the discontinuities, the two-layered approach and the loop concept in the NMM allow an easy crack identification and direct crack propagation simulation without further incorporating unknowns to the related nodes through enrichment functions. A detailed comparison between the NMM and other partition of unity methods was offered by Ma et al. (2009).

2.3.1. Crack identification and capture of strong discontinuities

To identify cracks in the NMM, the loop concept (Ning et al., 2011; Wu and Wong, 2012), on which the NMM contact technique is based, is employed. A loop is an independent closed domain, which can be either a block (an independent closed physical area) or a crack. As shown in Fig. 2, loop one is defined as the closed domain encompassed by outside boundary vertices, while loop two is defined as the closed domain encompassed by vertices from vertex 1 to vertex 14. As illustrated in the figure, the crack in the NMM has two faces: one is from vertex 1 to vertex 7, while the other one is from vertex 8 to vertex 14. This is how a closed pre-existing crack is defined in the NMM. When the crack intersects the MCs to form several PCs, each vertex that is on the crack, will be assigned to form different elements, as shown in Fig. 3. The other vertices that are related to the elements, which are not cut by the crack, will remain unchanged.

The PCs are then generated by the physical domains intersecting the MCs. As shown in Fig. 3(a), when the MC is cut completely by a crack into two sub-domains, two PCs are formed, e.g. P_1^1 and P_1^2. By the knowledge that "the elements in NMM are the common part of PCs", the original elements 1, 5 and 6 are divided into elements 7, 8, 9, 10, 11, 12, 13 and 14. Using the above procedures, the jump or discontinuity across the crack surface can be captured. For example, the jump across the surface between element 7 and element 11 can be expressed as:

$$[\![u^h]\!] = \sum_i \varphi_{i(ele\ 7)} u_{i(ele\ 7)} - \sum_j \varphi_{j(ele\ 11)} u_{j(ele\ 11)} \tag{2}$$

where $[\![\bullet]\!]$ represents the jump of a function; φ_i (i = 1, 2, 3) is the weight function associated with the corresponding PC; u_i (i = 1, 2, 3) is the local displacement function associated with the related PC.

However, for cases when the MC is partially cut by a crack, only one whole PC forms as P_1 in Fig. 3(b). Therefore, the discontinuity across the crack surface within element 4 cannot be captured by the conventional polynomial cover functions. To overcome this, some enrichment methods have been developed (Li and Cheng, 2005). In this study, the extrinsic enrichment method is adopted by directly adding the extrinsic basis which is extracted from the linear-elastic asymptotic displacement fields to the approximations through the partition

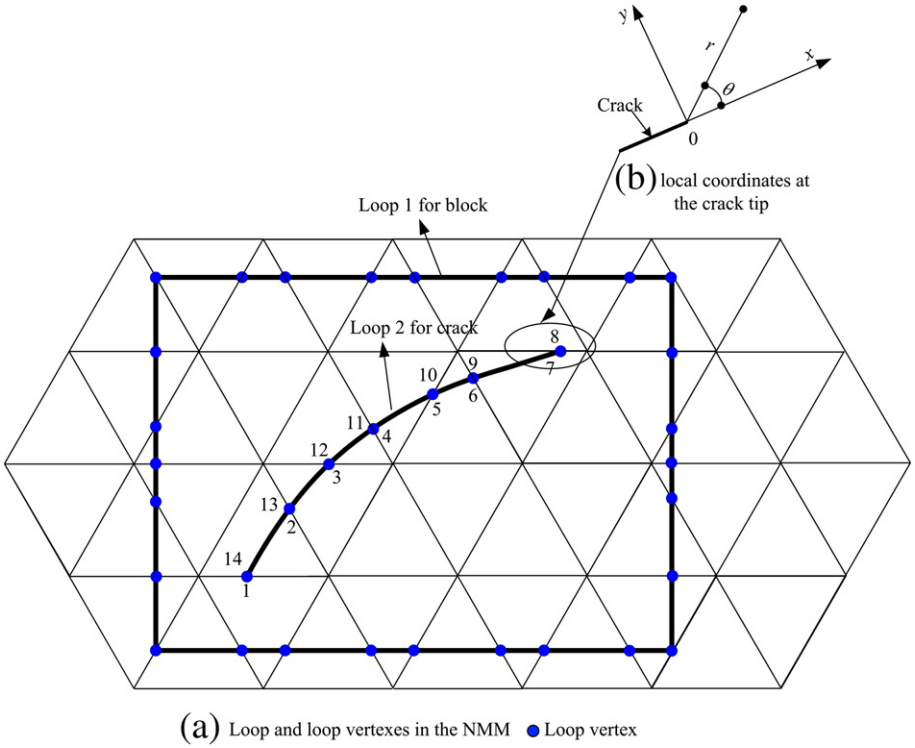

Fig. 2. Representations of loop, loop vertices and the local coordinates at the crack tip in the NMM (Ning et al., 2011; Wu and Wong, 2012).

of unity. The approximations in element 4 (Figure 3(c)) can then be expressed as:

$$u^h = \sum_i \varphi_i(x)\, u_i + \sum_i \varphi_i(x) \sum_j^4 k_i^j q_j(x) \tag{3}$$

where k_i^j are the enriched DOFs. $q_j\ (x)$ $(j = 1–4)$ is used to represent the local property at the crack tip and can be expressed as

$$\left[q_i^1, q_i^2, q_i^3, q_i^4\right] = \left[\sqrt{r}\sin\frac{\theta}{2}, \sqrt{r}\cos\frac{\theta}{2}, \sqrt{r}\sin\theta\sin\frac{\theta}{2}, \sqrt{r}\sin\theta\cos\frac{\theta}{2}\right]. \tag{4}$$

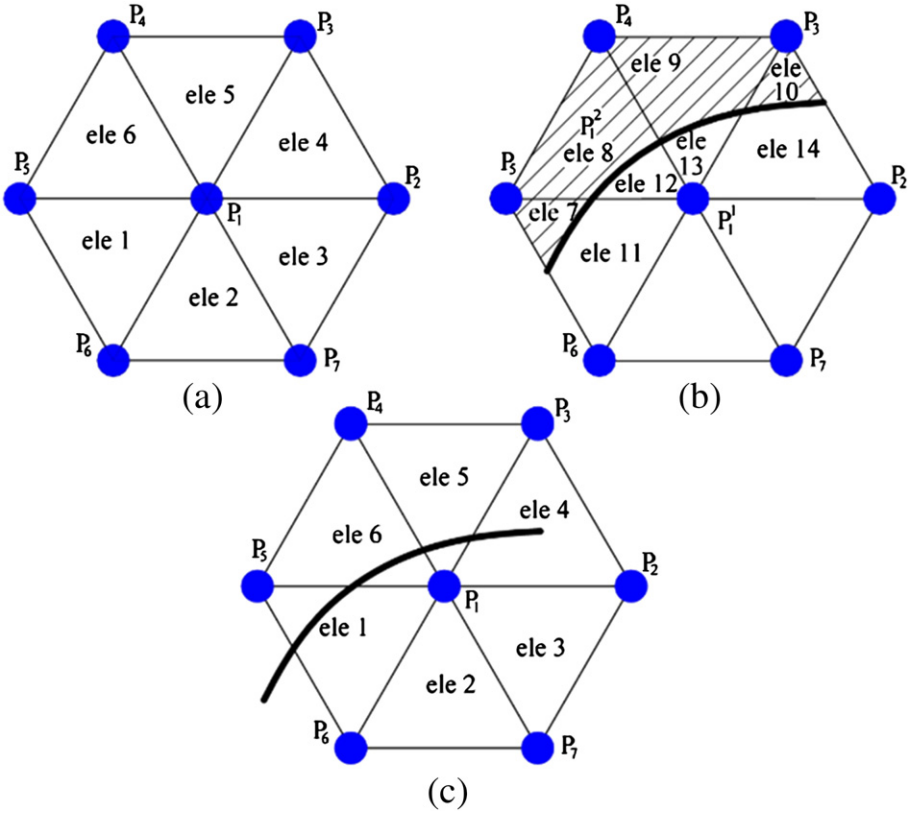

Fig. 3. Physical covers and elements (Ning et al., 2011; Wu and Wong, 2012) (a) before cracking, (b) after cracking for a fully-cut case and (c) after cracking for a partially-cut case.

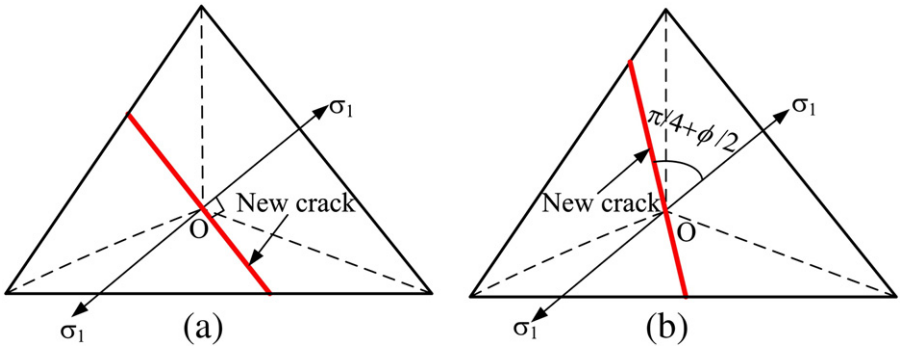

Fig. 4. Illustration of crack initiation for elements without crack tip. (a) Tensile crack and (b) shear crack (O represents the center of the elements) (Wu and Wong, 2013; Wu et al., 2013).

After the enrichment, as shown in Fig. 2, the upper crack surface has an angle θ_0 of π, while the bottom crack surface has an angle θ_0 of $-\pi$. Thus, the jump across the crack surfaces in element 4 (Figure 3) can be calculated as:

$$[\![u^h]\!] = 2\sqrt{r} \times \left(\varphi_1 k_1^1 + \varphi_2 k_3^1 + \varphi_3 k_3^1\right). \quad (5)$$

2.3.2. Treatment of manifold elements during cracking process

For the crack initiation case, when the elements without a crack tip satisfy the Mohr–Coulomb with cut-off failure criterion as discussed in Section 2.2, a macro-crack will initiate. However, with only the crack initiation direction determined by the failure criterion, the location of the crack is still indeterminate. As reported in our recent papers (Wu and Wong, 2012, 2013; Wu et al., 2013), we further assume that the crack passes through the center of the element. Then if the tensile strength of the material is reached, the development of a tensile macro-crack takes place with the crack direction perpendicular to σ_1, as shown in Fig. 4(a). If the shear failure strength of the material is reached, a shear macro-crack initiates at an angle of $(\pi / 4 + \phi / 2)$ with the direction of σ_1, as shown in Fig. 4(b).

Complications arise when an element contains one or more crack tips satisfying the failure criterion. Three different cases are described below. If an element containing one crack tip that reaches the failure criterion, the crack will propagate according to the predicted direction. If an element containing two crack tips that reaches the failure criterion, the newly formed crack is assumed to link the original two cracks together, as illustrated in Fig. 5(b). If an element containing more than two crack tips that reaches the failure criterion, the newly formed crack will link up the crack tips such that a minimum included angle θ_1 between the newly formed crack and the predicted crack propagation direction according to the failure criterion is achieved.

After crack initiation and propagation, the newly formed cracks then cut the MCs into certain sub-domains. The PCs and the manifold

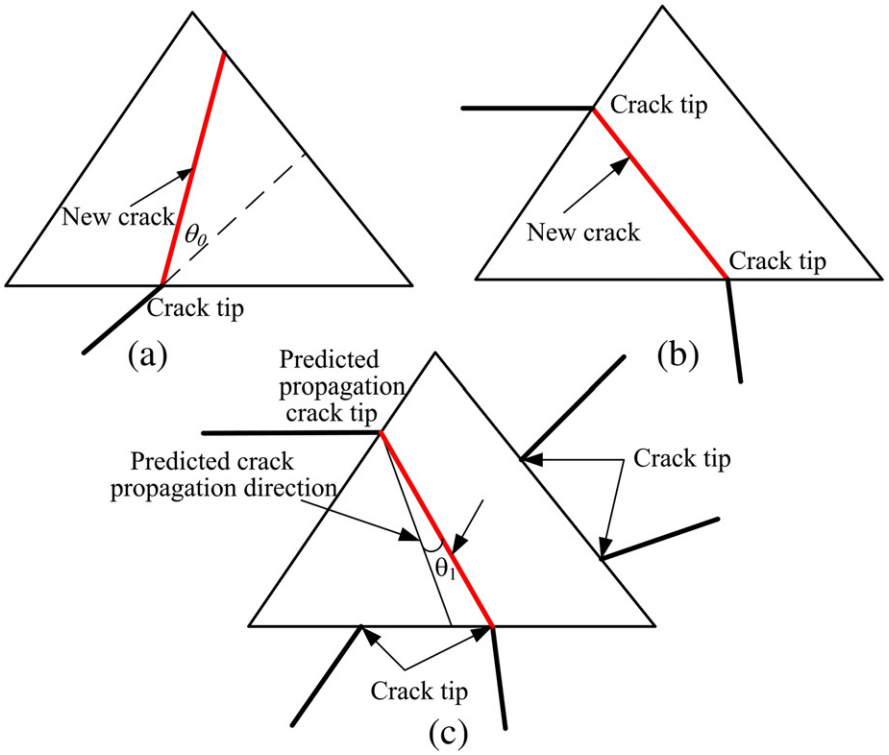

Fig. 5. Illustration of crack propagation in elements containing one or more crack tips. (a) Crack propagation in elements containing single crack tips; (b) newly formed crack in an element containing two crack tips; (c) linking the crack tips which have a minimum included angle θ_1 with the originally predicted crack trajectory in elements containing more than two crack tips (Wu and Wong, 2013; Wu et al., 2013).

elements will then update automatically according to the procedure discussed in Section 2.1.

2.3.3. Treatment of loops after crack initiation and propagation

In the NMM, the contact detection and crack representation are both based on loops. Therefore, once the crack initiation or propagation occurs, the loops need to be updated. Based on the relative position between the newly developed crack and the original loop, the modification to the loops can be categorized into the following four types (An, 2010; Ning et al., 2011; Wu and Wong, 2012). Type I: A new crack forms at an independent location without any intersection with the original loops, thus a new loop is added (Figure 6(a)). Type II: A new crack intersects the original loop, but it does not cut the loop into two parts. The new crack is added to the original loop (Figure 6(b)). Type III: A new crack cuts the original loop into two loops (Figure 6(c)). Type IV: A new crack combines the two original loops into a single loop (Figure 6(d)). Other types of loop updating can be deduced from the above four basic loop updating scenarios.

2.4. Treatment of weak discontinuity (material interface) in the NMM

In the traditional NMM, the material interface, which cuts the MCs into different parts, is treated the same as the strong discontinuity. To handle the displacement discontinuity across the material interface, additional techniques, such as the penalty method, the Lagrange multiplier method or the augmented Lagrange method are used (Kurumatani and Terada, 2009; Terada et al., 2003; Terada et al., 2007). However, these techniques require a longer time for iteration and sometimes even lead to diverging results.

In this paper, a more natural way to treat the material interfaces, which is adopted by XFEM (An et al., 2011; Sukumar et al., 2001), is employed. Instead of being split into two PCs, the PC which is fully cut by the material interface (weak discontinuity) keeps its integrity but its local displacement function is enriched. As shown in Fig. 7, the local functions for the PCs which are intersected by the material interfaces (PCs marked by solid circles) are enriched. The associated enrichment function is based on the level set function (Sukumar et al., 2001) identifying the location of the material interfaces. The level set function for the circular inclusions adopted in the present work is:

$$f(x) = \|x - x_c\| - r_c| \tag{6}$$

where x_c is the inclusion center and r_c is the inclusion radius. The interface is defined by $f(x) = 0$. Based on the level set function, several possible enrichment functions can be constructed, such as the absolute value of the level set function. However, a direct use of this function results in a convergence problems associated with blending elements as discussed by Fries (2008). Thus, a smoothing as suggested by Moes et al. (2003) is adopted, such that the enrichment function becomes

$$F(x) = \sum_i \varphi_i(x)|f_i| - \left|\sum_i \varphi_i(x) f_i\right|. \tag{7}$$

The above not only solves the convergence problem associated with blending elements, but also achieves a satisfactory convergence rate as discussed by Moes et al. (2003). As a result, the local displacement function for the PCs containing a weak discontinuity (material interface) becomes:

$$u(x) = \sum_i \varphi_i(x) \;\; (d_i + F(x)a_i) \tag{8}$$

where d_i, are the classical degrees of freedom, and a_i are the additional degrees of freedom.

3. Governing equations

In this section, the weak form and the discrete system of a linear elastic problem with a material interface treated by the NMM are presented.

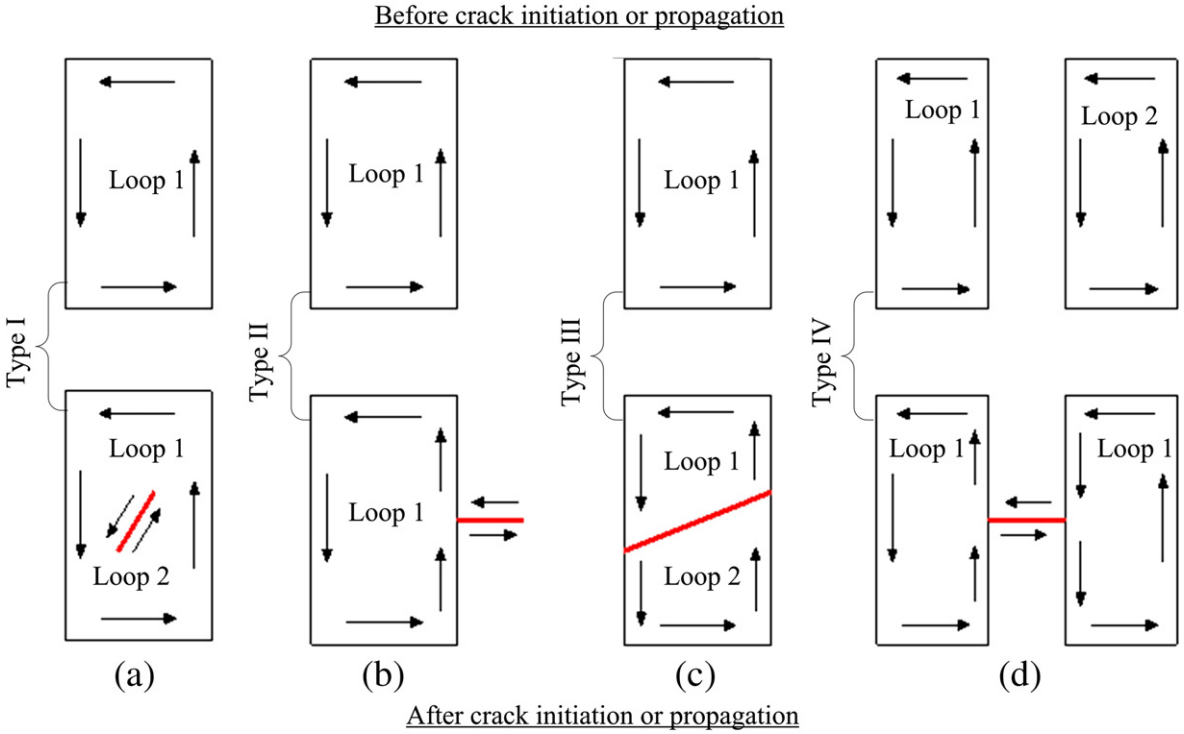

Fig. 6. Updating of loops after crack initiation and propagation: (a) Type I: a new loop forms, (b) Type II: a crack is added to the pre-existing loop, (c) Type III: the pre-existing loop is cut into two new loops, (d) Type IV: the pre-existing two loops combine into one (An, 2010; Ning et al., 2011; Wu and Wong, 2012).

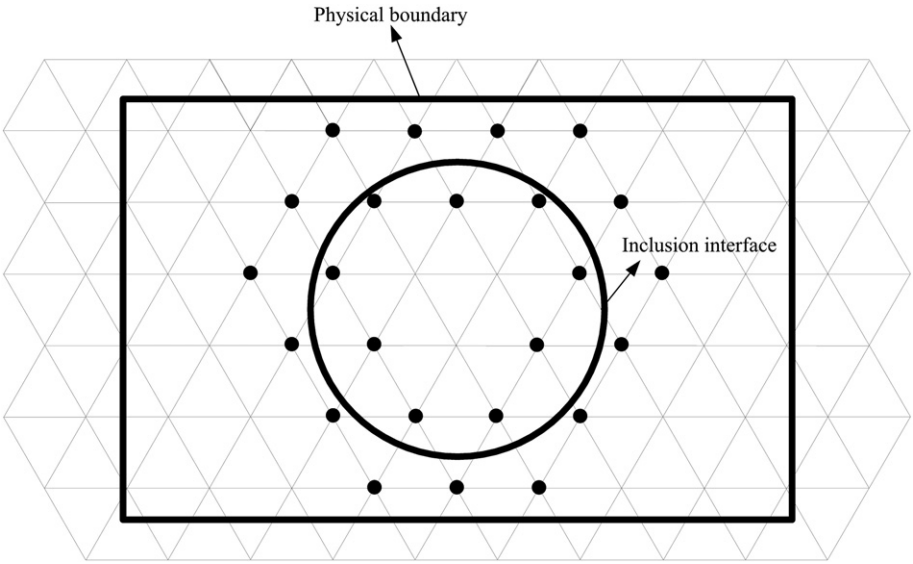

Fig. 7. Illustration of treatment of an inclusion in the NMM. PCs marked by solid circles are enriched by the interface enrichment function.

3.1. Weak form

Let u be the displacement solution for the stated linear elastostatic problem. Let $u \in V$ be the displacement trial function, and $\delta u \in V_0$ be any set of admissible test functions. The space $V = H_1(\Omega)$ is the Sobolev space of functions with square-integrable first derivatives in Ω and $V_0 = H^0{}_1(\Omega)$ is the Sobolev space functions with square-integrable first derivatives in Ω and vanishing values on the essential boundary Γ_u. The weak form of the governing equation and associated boundary conditions can be expressed as:

$$\int_{\Omega} \sigma(u) : \varepsilon(\delta u) d\Omega + \lambda \int_{\Gamma_u} (u - \overline{u}) \cdot \delta u d\Gamma = \int_{\Gamma_t} \overline{t} \cdot \delta u d\Gamma + \int_{\Omega} b : \varepsilon(\delta u) d\Omega \quad \forall \delta u \in V_0 \tag{9}$$

where σ and ε are stress and strain tensor, respectively. b is the body force and $\overline{u}$ and $\overline{t}$ are the essential boundary condition on Γ_u and traction boundary condition on Γ_t, respectively. λ is the real penalty number which is chosen to superimpose the essential boundary conditions.

3.2. Discrete system

In the NMM, finite-dimensional subspaces $V^h \subset V$ and $V_0^h \subset V_0$ are used as the approximating trial and test spaces. Using the Galerkin method (Lin, 2003), the weak form for the discrete problem can be stated as:

Find $u^h \in V^h \subset V$ such that

$$\int_{\Omega^h} \sigma\left(u^h\right) : \varepsilon\left(\delta u^h\right) d\Omega + \lambda \int_{\Gamma_u} \left(u^h - \overline{u}\right) \cdot \delta u^h d\Gamma = \int_{\Gamma_t} \overline{t} \cdot \delta u^h d\Gamma + \int_{\Omega^h} b \cdot \delta u^h d\Omega \quad \forall \delta u^h \in V_0^h \subset V_0. \tag{10}$$

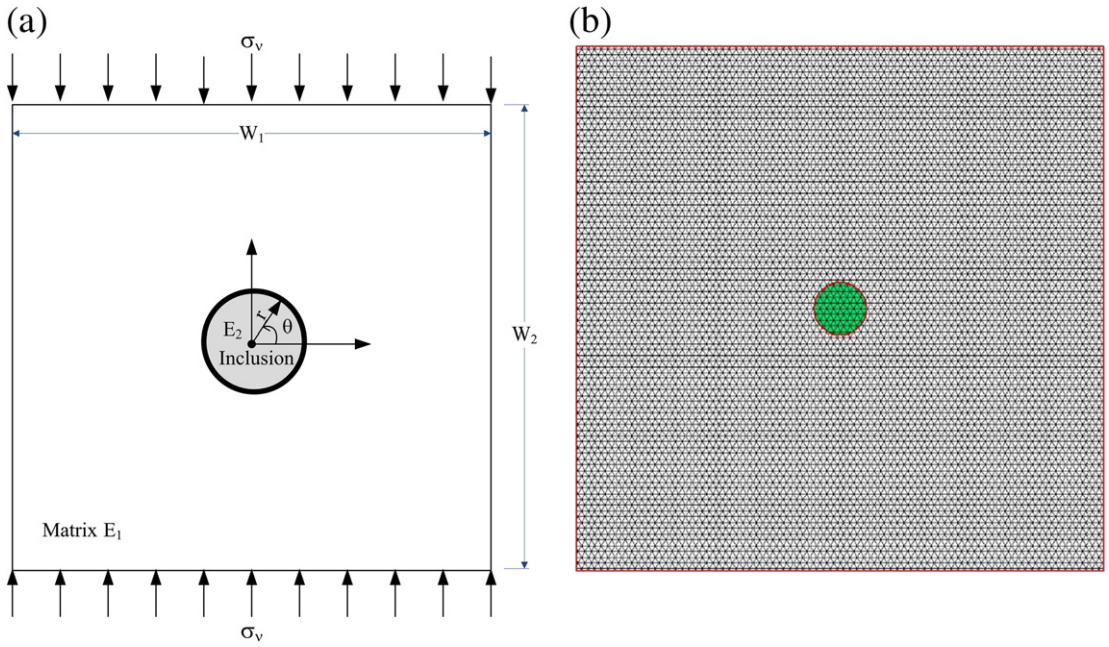

Fig. 8. A circular inclusion in an infinite plate under uniaxial compression. (a) Schematic illustration and (b) NMM model.

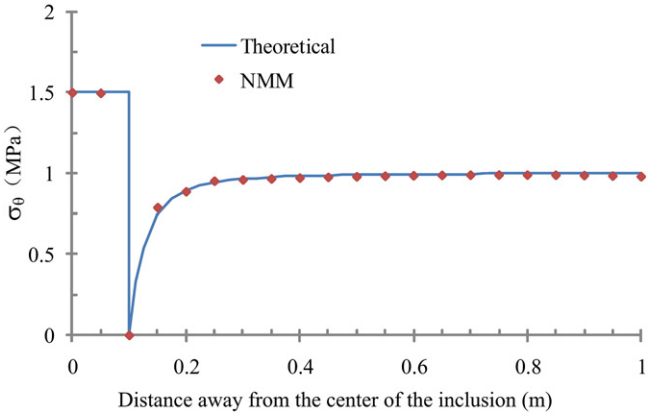

Fig. 9. σ_θ variation along direction of $\theta = 0$ for a rigid inclusion.

The trial function u^h as well as the test functions δu^h are expressed as

$$u^h(x) = \sum_i \varphi_i(x)(d_i + F(x)a_i) \tag{11}$$

$$\delta u^h(x) = \sum_i \varphi_i(x)(\delta d_i + F(x)\delta a_i). \tag{12}$$

Substituting the trial and test functions from Eqs. (11) and (12) into Eq. (10), and using the arbitrariness of the test functions, the following discrete system is obtained:

$$\mathrm{Kd} = \mathrm{f} \tag{13}$$

where

$$K_{ij} = \int_{\Omega^h} B_i^T D B_j d\Omega + \lambda \int_{\Gamma_u} (\varphi_i)^T \cdot \left(\varphi_j\right) d \tag{14}$$

$$f_i = \int_{\Gamma_t^h} \widehat{\phi}_i \cdot \bar{t} d\Gamma + \int_{\Omega^h} \widehat{\phi}_i \cdot b d\Omega + \lambda \int_{\Gamma_t^h} \widehat{\phi}_i \cdot \bar{u} d\Gamma \tag{15}$$

where $\widehat{\phi}_i \equiv \varphi_i$ for a finite-element displacement degree of freedom, and $\widehat{\phi}_i \equiv \varphi_i F$ for an enriched degree of freedom. D is the constitutive matrix for an isotropic linear elastic material, and the matrix B_i is:

$$B_i = \begin{bmatrix} \widehat{\phi}_{i,x} & 0 \\ 0 & \widehat{\phi}_{i,y} \\ \widehat{\phi}_{i,y} & \widehat{\phi}_{i,x} \end{bmatrix}.$$

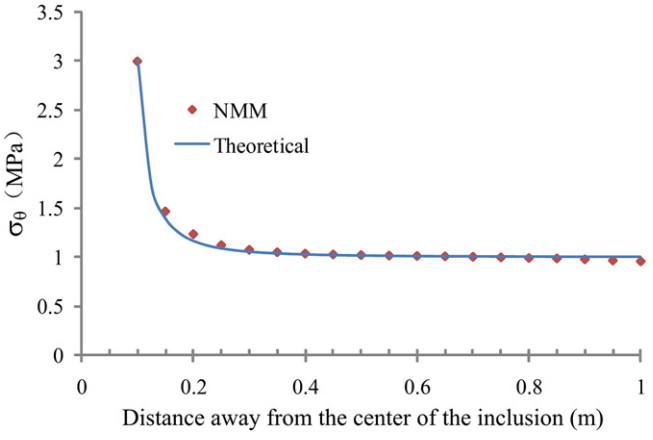

Fig. 10. σ_θ variation along direction of $\theta = 0$ for a hole.

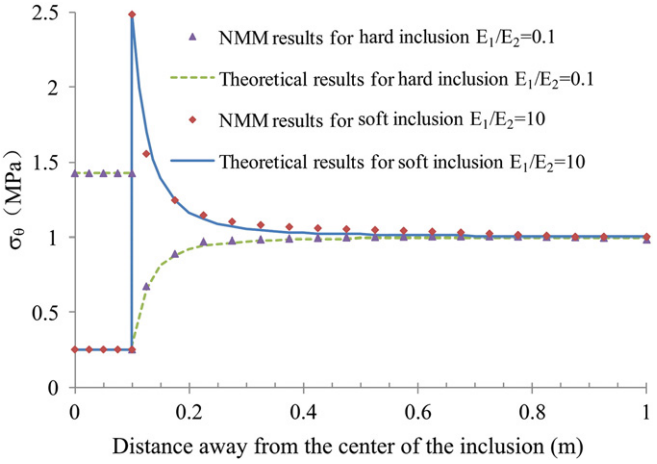

Fig. 11. σ_θ variation along direction of $\theta = 0$ for different stiffness ratios.

4. Numerical results

When a specimen containing an inclusion is loaded, cracking occurs at the location of the largest tensile or shear stress concentration when the Mohr–Coulomb strength of the material at that point is exceeded. Since the inclusion and matrix typically have different mechanical properties, especially the modulus of elasticity, thermal coefficient, and hardening rate in addition to strength (Mitsui et al., 1994), it is, therefore, important to understand if any stress concentrations develop at the interface because of these mechanical differences. Under the linear elastic assumption, the property that has the greatest influence on the internal stress distribution in a composite material is the difference between the elastic constants of the inclusion and the surrounding matrix (Neville, 1997).

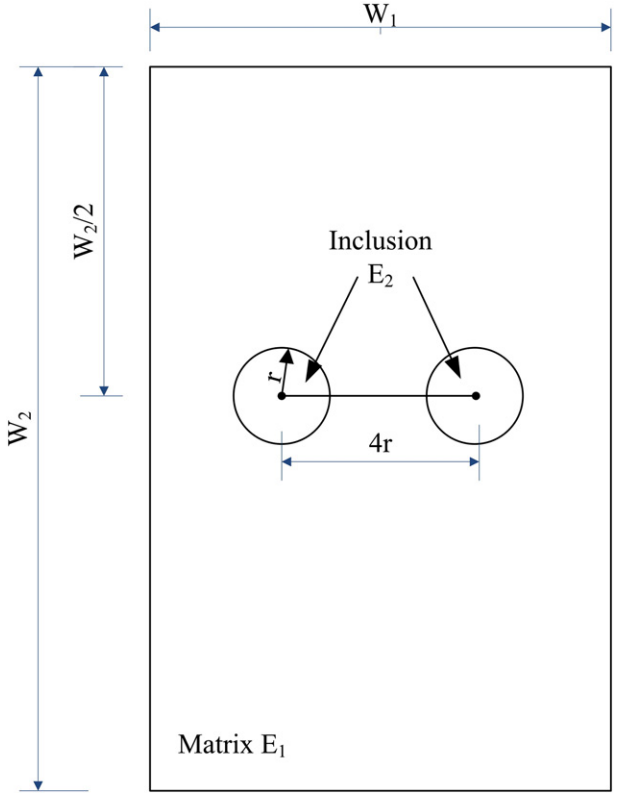

Fig. 12. Physical model of specimen containing double inclusions.

Table 1
Material properties of numerical simulation (Janeiro, 2009).

	Hydrocal® matrix	Ultracal® inclusion	Plaster inclusion
Young's modulus E (GPa)	15.0	29	10.5
Poisson ratio ν	0.25	0.25	0.25
Tensile strength σ_t (MPa)	−2.4	−3.9	−2.9
Compressive strength σ_0 (MPa)	37.2	91.1	28.6

In this section, before using the developed NMM to analyze the cracking behavior associated with a plate containing one or two circular inclusions with different stiffness under compression, we first verify the capability of the developed NMM in capturing the weak discontinuity across the interface. Then the cracking events (crack initiation and propagation), crack mechanisms (tensile or shear) and the coalescence processes associated with an inclusion and its surrounding matrix are investigated in specimens containing either one or two inclusions.

4.1. Verification of the developed NMM in capturing the weak discontinuity

A plate containing a circular inclusion under a uniaxial compression as shown in Fig. 8 is studied for the verification purpose. The dimensions of the plate are $W_1 = W_2 = 2$ m. The radius (r) of the inclusion is 0.1 m. The Possion's ratio (ν) of both the plate and the inclusion is 0.25, and the Young's modulus of the plate E_1 and that of the inclusion E_2 are 1 MPa and varied respectively. A mesh with 7538 MCs, 7490 common PCs, 48 enriched PCs and 14,678 manifold elements is selected. Four cases of different stiffness ratios between the plate and the inclusion E_1/E_2 are considered, including soft inclusion problems with $E_1/E_2 = 10$ and a hole $E_2 = 0$, and stiff inclusion problems with $E_1/E_2 = 0.1$ and a rigid inclusion $E_2 = \infty$.

By sampling the measurement points along the direction of $\theta = 0$ from the center of the inclusion to the edge of the plate at an interval of 0.05 m, the circumferential stresses σ_θ at the measurement points due to different inclusion stiffness are obtained and compared with the theoretical results as shown in Figs. 9, 10 and 11. As illustrated

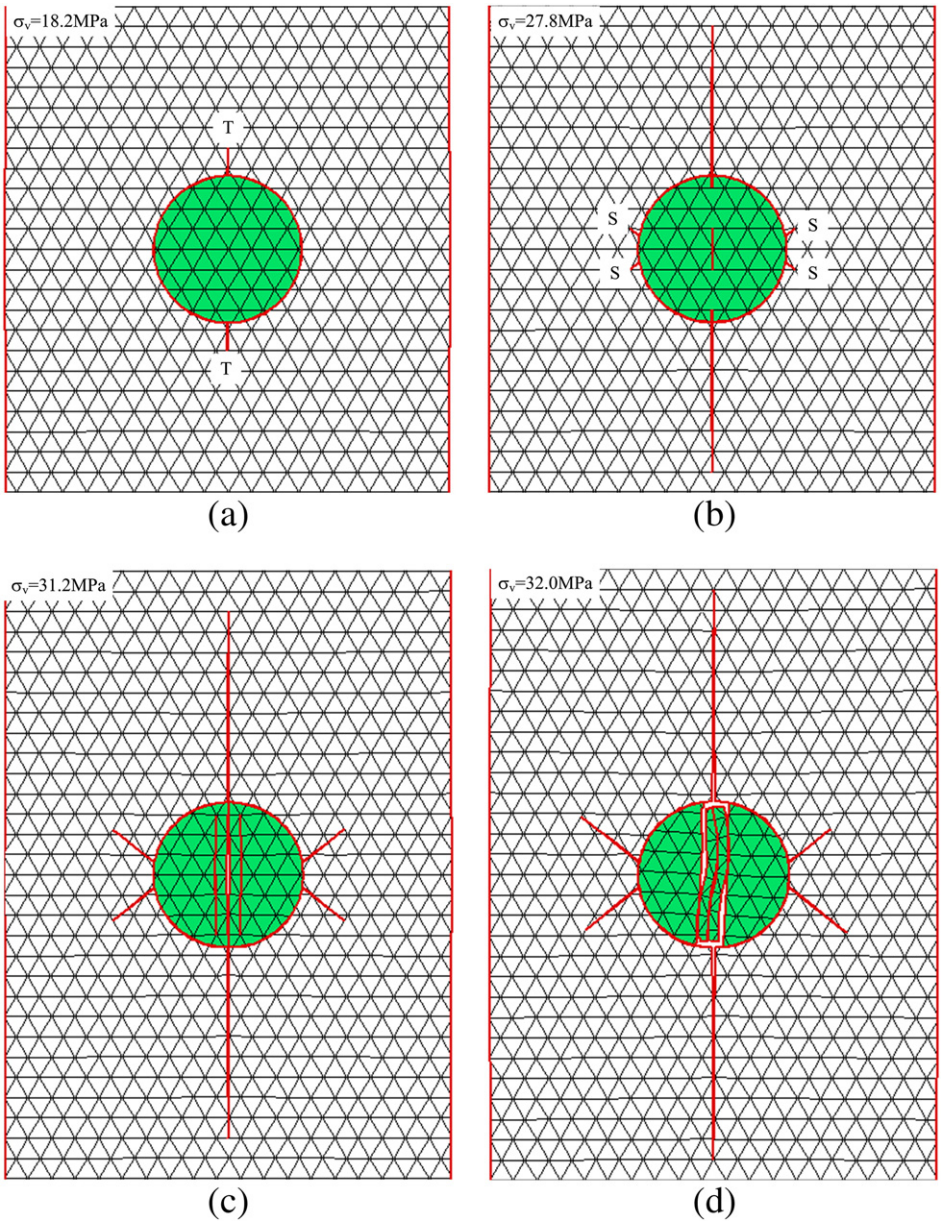

Fig. 13. Crack sequences for the weak (Plaster) single inclusion obtained by NMM. T = tensile crack, S = shear crack. (a) Initiation of first tensile cracks, (b) initiation of shear cracks, (c) status before coalescence and (d) status at maximum stress.

in the figures, by incorporating the enriched method to treat the weak discontinuity, the NMM can accurately capture the stress discontinuity (weak discontinuity) across the interface for inclusions with varied stiffness. In particular, for soft inclusions, the maximum stress concentration appears at the interface along the direction of $\theta = 0$ (and $\theta = \pi$). For hard inclusions, instead of the stress concentration that occurred at the interface along the direction of $\theta = 0$ (and $\theta = \pi$), a stress dissipation is obtained.

4.2. Numerical prediction

4.2.1. Background

Based on the enriched method to treat the material interface, the Mohr–Coulomb crack initiation criterion, and the crack treating technique, the cracking behavior of specimens containing single or double inclusions under uniaxial compression is numerically studied by the developed NMM. The crack initiation and propagation in specimens containing single inclusions with varied stiffness are first studied, which is followed by an investigation of the crack coalescence of double inclusions with low stiffness. The relevant predictions obtained from the NMM are compared with the physical experimental results obtained by Janeiro (2009) and Janeiro and Einstein (2010). Details of the cracking mechanism (tensile/shear) and the entire cracking sequence, which are captured by the high speed video technology (Wong and Einstein, 2009), allow us to validate the capability of the developed method in predicting the cracking behavior.

The dimensions of the numerical model are the same as those of the physical models adopted by Janeiro (2009), which have a width W_1 of 76.2 mm, a length W_2 of 152.4 mm. The radius of the inclusion is 12.7 mm for single inclusion (as shown in Figure 8) and 6.35 mm for double inclusions (as shown in Figure 12). For the single inclusion problem, a mesh with 1668 MCs, 1632 common PCs, 36 enriched PCs and 3110 manifold elements is selected, while for the double inclusion problem, a mesh with 1674 MCs, 1634 common PCs, 40 enriched PCs and 3116 manifold elements is selected. The material properties are listed in Table 1. The Ultracal® and Plaster represent the stiff and weak inclusions respectively.

4.2.2. Single inclusion

Fig. 13 presents typical cracking sequences and the respective applied stress σ_v at each status predicted by the NMM in a specimen containing a single weak (plaster) inclusion under uniaxial vertical

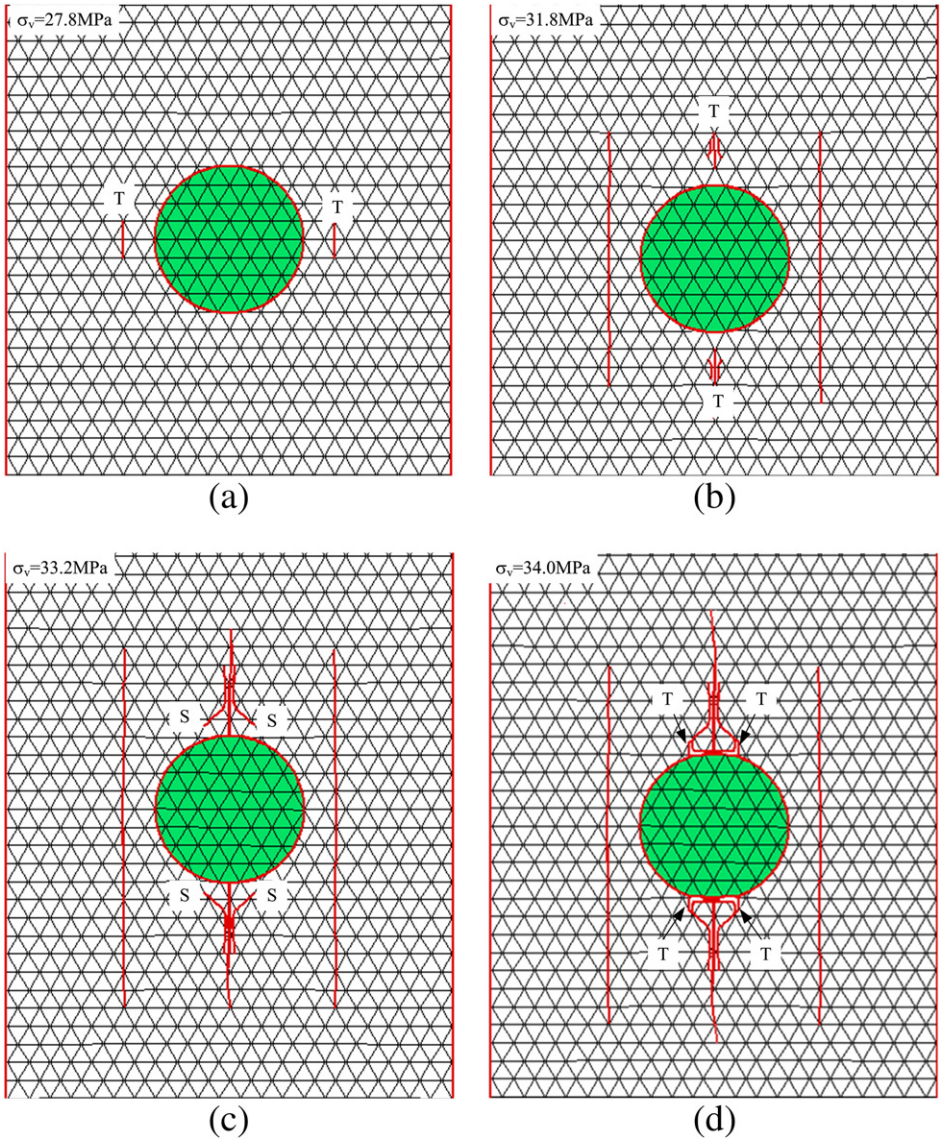

Fig. 14. Crack sequences for the stiff (Ultracal®) single inclusion obtained by NMM. T = tensile crack, S = shear crack. (a) Initiation of first tensile cracks, (b) initiation of secondary tensile cracks, (c) status before coalescence and (d) status at maximum stress.

loading. As demonstrated in the figure, the cracking behavior can be categorized into the following stages. First, vertical tensile cracks initiate at the top and bottom of the interface and propagate to the direction of the external load (Figure 13a). As the load increases, shear cracks initiate at the two sides (beside $\theta = 0$) of the interface and additional tensile cracks initiate within the inclusion (Figure 13b). As the load continues to increase, the previously developed cracks keep on propagating. Particularly the central tensile crack initiated within the inclusion reaches the interface and coalesces with the earlier initiated tensile cracks (Figure 13c). Finally, the specimen fails when the maximum stress is reached (Figure 13d). These cracking processes are in general good agreement with the experimental results obtained by Janeiro (2009), as shown in Fig. 15a. Observe that the crack initiation stress and maximum stress predicted by the NMM are 18.2 MPa and 32.0 MPa respectively, which are only 9% and 6% different from the physical results of 20.0 MPa and 34.0 MPa. Considering the inherent uncertainty and randomness of the modeled rock properties, the prediction by the NMM simulation is deemed acceptable.

Similarly, the cracking sequences in a specimen containing a stiff inclusion (Ultracal®) obtained from the NMM and experiments are presented in Figs. 14 and 15b respectively. As illustrated in the figures, for both models, tensile cracks first initiate in the interior of the matrix instead of from the inclusion interface. This can be explained by the theoretical results shown in Fig. 16, from which the maximum tensile stress is found to occur in the interior of the matrix, but a short distance away from the interface. The different locations of the first cracks in numerical and physical tests may be caused by the loading condition, particularly the edge effect. After these first tensile cracks have propagated for several steps, several new tensile cracks initiate at a distance away from the top and bottom of the interface in the numerical model (Figure 14b), while in the physical test, debonding along the interface occurs prior to the initiation of new tensile cracks. When the load increases, in the numerical model, the previously developed cracks keep on propagating until those cracks above and below the inclusion reach the interface (Figure 14c, d). In the physical test, after debonding, tensile cracks and shear cracks, which are similar to those observed in the specimen containing a weak inclusion as shown in Fig. 13, develop. This discrepancy between the numerical and physical test results could be caused by the debonding which is generally observed during the physical tests. Although the enriched method used in this paper can successfully capture the weak discontinuity across the interface, there is still

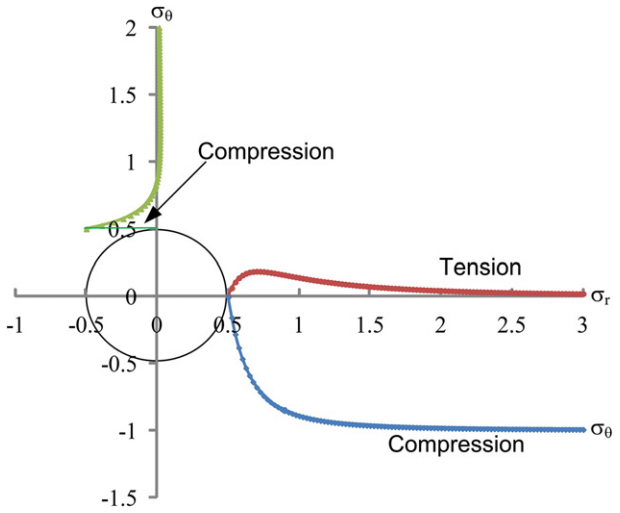

Fig. 16. The tangential σθ and radial σr stress concentration factors for a stiff inclusion (E2/E1 = 2). (Compression is negative and tension is positive).

a discrepancy between the numerically modeled interface and the real grain interface. Except the weak discontinuity across the interface, the elements containing the interface are the same as the other perfect elements. Therefore, the enriched method is hard to capture the debonding along the interface. After debonding, the stiff inclusion becomes more like a hole which makes the subsequent cracking behavior similar to that of a weak inclusion. Note also that the crack initiation stress and the maximum stress predicted by the NMM are 27.8 MPa and 34.0 MPa respectively, which are only 4.1% and 6.3% different from the physical results of 29.0 MPa and 32.0 MPa.

4.2.3. Double inclusions

The cracking sequences and respective applied stresses in a specimen containing double weak inclusions obtained from the NMM are presented in Fig. 17. As shown in the figure, when the applied stress is smaller than 29.6 MPa, the cracking behavior of the double inclusions behaves similar to that of the single inclusion (Figure 13). First, tensile cracks initiate at the top and bottom of the interfaces (Figure 17a). Later, additional tensile cracks initiate at the center of

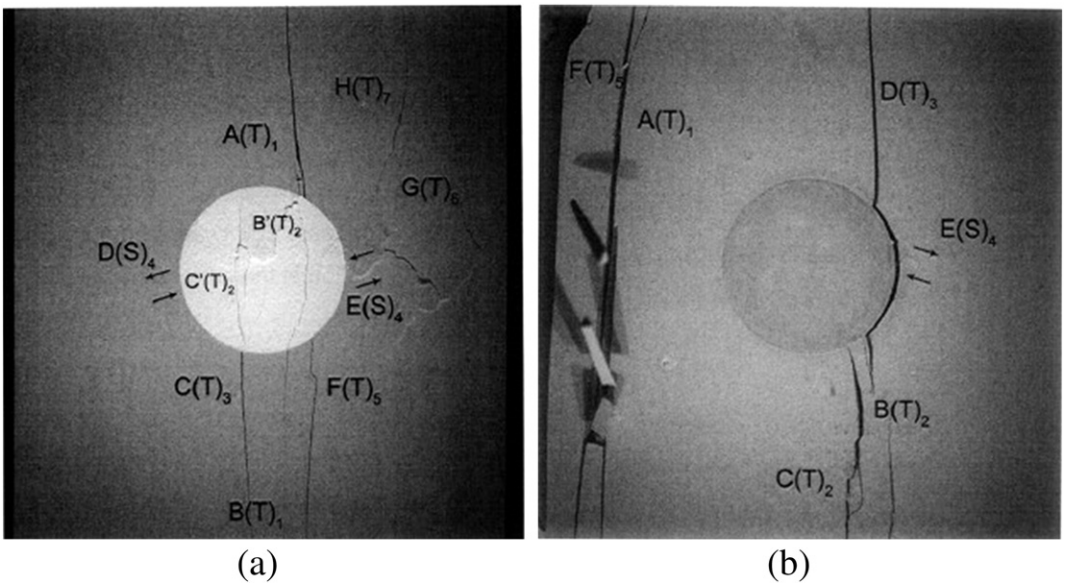

Fig. 15. Physical test results of hydrocal specimens containing a single inclusion. (a) Plaster inclusion and (b) Ultracal® inclusion (Janeiro, 2009). All the identifiable new cracks are identified by reference letters, e.g., B, C, etc. Each letter is then followed a letter T or S in parentheses, which refers to either the tensile mode or the shear mode of crack initiation, respectively. The sequence of crack initiation is indicated by numbers shown as subscripts. The first crack to initiate is designated as 1, the second crack as 2, etc (Wong and Einstein, 2009).

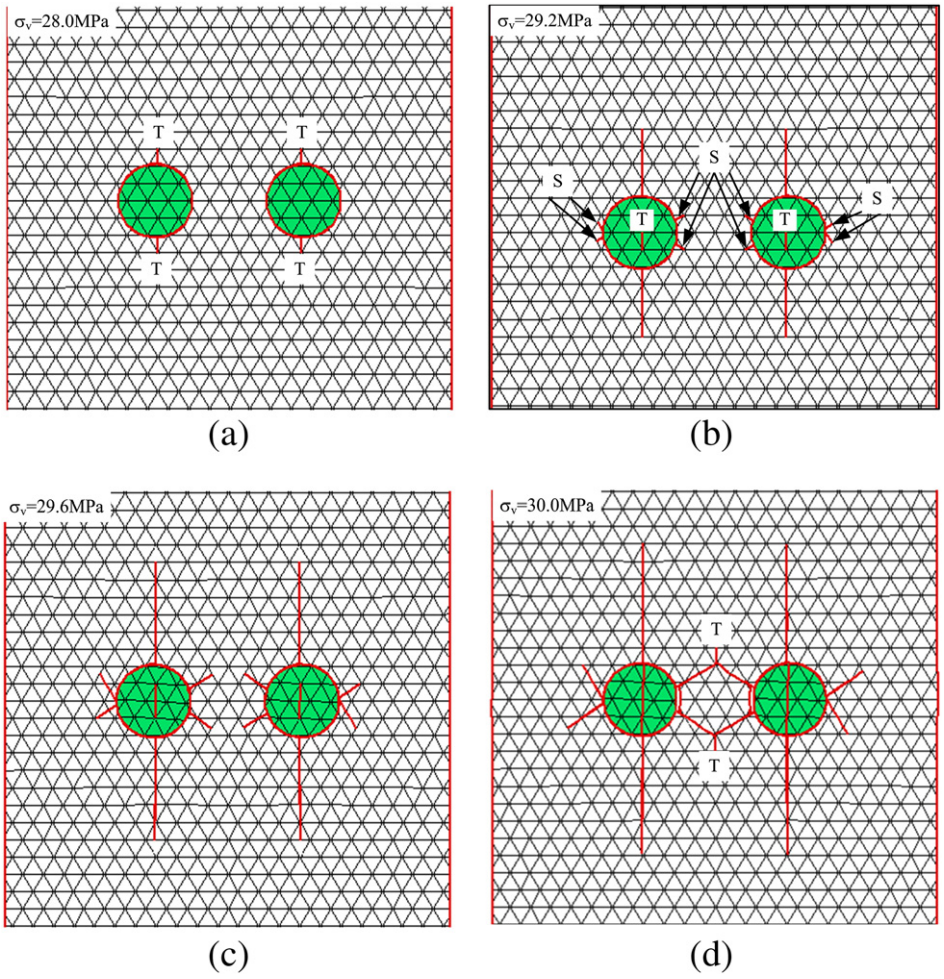

Fig. 17. Crack sequences for the weak (Plaster) double inclusions obtained by NMM. T = tensile crack, S = shear crack. (a) Initiation of first tensile cracks, (b) initiation of shear cracks (c) status before shear coalescence and (d) status at maximum stress.

the inclusions and shear cracks initiate at the two sides of the interfaces (Figure 17b, c). However, as the applied load further increases (σ_v = 29.6 MPa), the previously developed neighboring shear cracks emanating from the two interfaces coalesce. After the coalescence, two new tensile cracks initiate at the junctions of the coalesced shear cracks and the cracks at the side of both interfaces open, during which the maximum applied stress reaches.

Compared with the experimental result shown in Fig. 18, the NNM combined with the enriched method can predict not only the simple cracking behavior (crack initiation and propagation) for double weak inclusions, but also the complex cracking behavior (crack coalescence). The final mode of specimen failure is successfully predicted as well. The crack initiation stress and the maximum stress predicted by the NMM are 28.0 MPa and 32.0 MPa respectively, which are only 7.6% and 4.3% different from the physical results of 30.32 MPa and 30.64 MPa.

5. Conclusions

In the present study, the NMM has been extended to investigate the cracking behavior of specimens containing either one or double inclusions under uniaxial compression. We incorporated the enriched method as presented by XFEM into the NNM framework to treat the weak discontinuities across the material interfaces. Based on the superiorities of the NMM in dealing with the strong discontinuities and the incorporation of the crack initiation and propagation criteria,

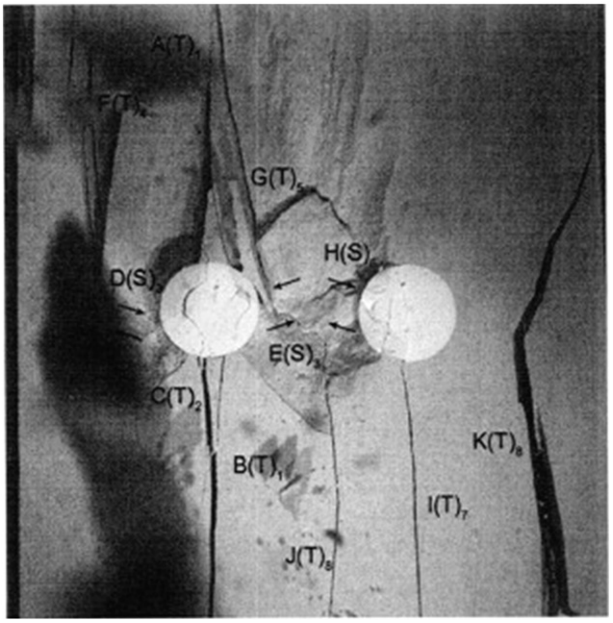

Fig. 18. Physical test results of hydrocal specimen containing double weak inclusions (Janeiro, 2009).

the crack identification method and the crack evolution technique, the cracking processes (cracking initiation, propagation and coalescence, the mechanism of the developed crack) are successfully modeled. For validating the efficiency of the proposed method, the numerical results are compared with both the theoretical and physical test results, based on which the following conclusions can be drawn:

1. By adopting a two-cover system, the NMM can easily capture the strong discontinuity between the crack surfaces in a direct way without further incorporating enrichment functions for most cases, which is typically necessary for other partition of unity methods.
2. With the crack identification method and crack evolution technique, the NMM is able to model not only simple cracking problems (single crack initiation and propagation) but also crack coalescence problems.
3. The enriched method proposed to treat the material discontinuities within the NMM framework is shown to be powerful to capture the weak discontinuities across the interfaces for varied stiffness ratio. Since the enriched method treats the material discontinuities in a natural way, no additional PCs and manifold elements are formed, as well as no additional iterations are induced by enforcing the displacement compatibility condition for as in other penalty weak discontinuity methods.
4. The comparisons between the numerical results and the physical tests (Janeiro, 2009) reveal that by incorporating the proposed enriched method and the crack treating techniques, the NNM can successfully predict the cracking behavior such as crack initiation stress, peak stress and crack type in specimens containing either single or double weak inclusions. However, the proposed enriched method still cannot realistically represent the material interface. Although it can successfully capture the stress discontinuities across the interface, no "real" interface exists in the NMM treatment. As a result, the debonding phenomenon which is frequently observed in physical tests is hard to be captured by the proposed method. Since after debonding, the inclusion behaves like a hole (similar to weak inclusion), the proposed method cannot satisfactorily predict the cracking behavior in specimens containing stiff inclusions.

Acknowledgments

The research was supported by the Academic Research Fund Tier 1 (RG19/10) and the Nanyang Technological University Start Up Grant (M4080115.030). The authors would also like to thank Dr Gen-Hua Shi, Dr Youjun Ning and Professor Guowei Ma for valuable discussion, which inspired the authors to conduct the present research.

References

An, X.M., 2010. Extended numerical manifold methods for engineering failure analysis. Civil and Environmental Engineering,Nanyang Technology University Singapore.
An, X.M., Ma, G.W., Cai, Y.C., Zhu, H.H., 2011. A new way to treat material discontinuities in the numerical manifold method. Computer Methods in Applied Mechanics and Engineering 200, 3296–3308.
Babuska, I., Melenk, J.M., 1997. The partition of unity method. International Journal for Numerical Methods in Engineering 40, 727–758.
Belytschko, T., Black, T., 1999. Elastic crack growth in finite elements with minimal remeshing. International Journal for Numerical Methods in Engineering 45, 601–620.
Belytschko, T., Lu, Y.Y., Gu, L., 1994. Element-free galerkin methods. International Journal for Numerical Methods in Engineering 37, 229–256.
Belytschko, T., Moes, N., Usui, S., Parimi, C., 2001. Arbitrary discontinuities in finite elements. International Journal for Numerical Methods in Engineering 50, 993–1013.
Bouchard, P.O., Bay, F., Chastel, Y., 2003. Numerical modelling of crack propagation: automatic remeshing and comparison of different criteria. Computer Methods in Applied Mechanics and Engineering 192, 3887–3908.
Brady, B., Brown, E., 1993. Rock Mechanics for Underground Mining, 2nd ed. Chapama&Hall, London, UK.
Chiou, Y.J., Lee, Y.M., Tsay, R.J., 2002. Mixed mode fracture propagation by manifold method. International Journal of Fracture 114, 327–347.
Cotterell, B., Rice, J.R., 1980. Slightly curved or kinked cracks. International Journal of Fracture 16, 155–169.
Erdogan, F., Sih, S.C., 1963. On the crack extension in plates under plane loading and transverse shear. Journal of Basic Engineering ASME 85, 519–525.
Fries, T.P., 2008. A corrected XFEM approximation without problems in blending elements. International Journal for Numerical Methods in Engineering 75, 503–532.
Hussian, M.A., PU, Underwood, J., 1974. Strain energy release rate for a crack under combined mode I and mode II. Fracture analysis ASTM STP, 560, pp. 2–28.
Janeiro, R.P., 2009. The Effect of Inclusion In Brittle Material, Civil and Environmental Engineering. Massachusetts Institute of Technology, Cambridge.
Janeiro, R.P., Einstein, H.H., 2010. Experimental study of the cracking behavior of specimens containing inclusions (under uniaxial compression). International Journal of Fracture 164, 83–102.
Khan, S.M.A., Khraisheh, M.K., 2000. Analysis of mixed mode crack initiation angles under various loading conditions. Engineering Fracture Mechanics 67, 397–419.
Kurumatani, M., Terada, K., 2009. Finite cover method with multi-cover layers for the analysis of evolving discontinuities in heterogeneous media. International Journal for Numerical Methods in Engineering 79, 1–24.
Li, S.C., Cheng, Y.M., 2005. Enriched meshless manifold method for two-dimensional crack modeling. Theoretical and Applied Fracture Mechanics 44, 234–248.
Lin, J.S., 2003. A mesh-based partition of unity method for discontinuity modeling. Computer Methods in Applied Mechanics and Engineering 192, 1515–1532.
Ma, G.W., An, X.M., Zhang, H.H., Li, L.X., 2009. Modeling complex crack problems using the numerical manifold method. International Journal of Fracture 156, 21–35.
Melenk, J.M., Babuska, I., 1996. The partition of unity finite element method: basic theory and applications. Computer Methods in Applied Mechanics and Engineering 139, 289–314.
Mitsui, K., Li, Z.J., Lange, D.A., Shah, S.P., 1994. Relationship between microstructure and mechanical properties of the paste–aggregate interface. ACI Materials Journal 91, 30–39.
Moes, N., Dolbow, J., Belytschko, T., 1999. A finite element method for crack growth without remeshing. International Journal for Numerical Methods in Engineering 46, 131–150.
Moes, N., Cloirec, M., Cartraud, P., Remacle, J.F., 2003. A computational approach to handle complex microstructure geometries. Computer Methods in Applied Mechanics and Engineering 192, 3163–3177.
Neville, A.M., 1997. Aggregate bond and modulus of elasticity of concrete. ACI Materials Journal 94 (1), 71–74.
Nielsen, C.V., Legarth, B.N., Niordson, C.F., 2012. Extended FEM modeling of crack paths near inclusions. International Journal for Numerical Methods in Engineering 89, 786–804.
Ning, Y.J., An, X.M., Ma, G.W., 2011. Footwall slope stability analysis with the numerical manifold method. International Journal of Rock Mechanics and Mining Sciences 48, 964–975.
Rabczuk, T., Belytschko, T., 2004. Cracking particles: a simplified meshfree method for arbitrary evolving cracks. International Journal for Numerical Methods in Engineering 61, 2316–2343.
Rabczuk, T., Areias, P.M.A., Belytschko, T., 2007. A simplified mesh-free method for shear bands with cohesive surfaces. International Journal for Numerical Methods in Engineering 69, 993–1021.
Rashid, M.M., 1998. The arbitrary local mesh replacement method: an alternative to remeshing for crack propagation analysis. Computer Methods in Applied Mechanics and Engineering 154, 133–150.
Shi, G.H., 1991. Manifold method of material analysis. Trans 9th Army Conf on Applied Mathematics and Computing, Minneapolis: Minnesota, pp. 57–76.
Shi, G.H., 1992. Modeling rock joints and blocks by manifold method. Proceedings of the 33th US Rock Mechanics Symposium, New Mexico: Santa Fe, pp. 639–648.
Shi, G.H., Goodman, R.E., 1989. Generalization of two-dimensional discontinuous deformation analysis for forward modeling. International Journal for Numerical and Analytical Methods in Geomechanics 13, 359–380.
Sih, G.C., 1974. Strain-energy-density factor applied to mixed crack problems. International Journal of Fracture 10, 305–321.
Strouboulis, T., Babuska, I., Copps, K.L., 2000. The design and analysis of the Generalized Finite Element Method. Computer Methods in Applied Mechanics and Engineering 181, 43–69.
Strouboulis, T., Copps, K., Babuska, I., 2000. The generalized finite element method: an example of its implementation and illustration of its performance. International Journal for Numerical and Analytical Methods in Geomechanics 47 (8), 1401–1417.
Sukumar, N., Chopp, D.L., Moës, N., Belytschko, T., 2001. Modeling holes and inclusions by level sets in the extended finite-element method. Computer Methods in Applied Mechanics and Engineering 190, 6183–6200.
Terada, K., Asal, M., Yamagishi, M., 2003. Finite cover method for linear and non-linear analyses of heterogeneous solids. International Journal for Numerical Methods in Engineering 58, 1321–1346.
Terada, K., Ishii, T., Kyoya, T., Kishino, Y., 2007. Finite cover method for progressive failure with cohesive zone fracture in heterogeneous solids and structures. Computational Mechanics 39, 191–210.
Trädegård, A., Nilsson, F., Östlund, S., 1998. FEM-remeshing technique applied to crack growth problems. Computer Methods in Applied Mechanics and Engineering 160, 115–131.
Tsay, R.J., Chiou, Y.J., Chuang, W.L., 1999. Crack growth prediction by manifold method. Journal of Engineering Mechanics—ASCE 125, 884–890.
Wong, L.N.Y., Einstein, H.H., 2009. Using high speed video imaging in the study of cracking processes in rock. Geotechnical Testing Journal 32, 164–180.
Wu, Z., Wong, L.N.Y., 2012. Frictional crack initiation and propagation analysis using the numerical manifold method. Computer and Geotechnics 39, 38–53.
Wu, Z., Wong, L.N.Y., 2013. Elastic–plastic cracking analysis for brittle–ductile rocks using manifold method. International Journal of Fracture 180 (1), 71–91.
Wu, Z., Wong, L.N.Y., Fan, L.F., 2013. Dynamic study on fracture problems in viscoelastic sedimentary rocks using the numerical manifold method. Rock Mechanics and Rock Engineering. http://dx.doi.org/10.1007/s00603-012-0349-4 (available online).